Proceedings of IMECE2005
2005 ASME International Mechanical Engineering Congress and Exposition
November 5-11, 2005, Orlando, Florida USA

IMECE2005-81318

AERO ELASTIC FLUTTER AT THE FREE EDGES OF UNI-AXIALLY TENSIONED WEBS AND THIN FILMS

Rahul A. Bidkar***
Graduate Student
rbidkar@purdue.edu

Arvind Raman
Associate Professor
raman@ecn.purdue.edu

Anil K. Bajaj
Professor
bajaj@ecn.purdue.edu

Dynamic Systems and Stability Laboratory
School of Mechanical Engineering
Purdue University
West Lafayette, IN-47907
*** corresponding author

ABSTRACT

Aero elastic flutter may play an important role in the breakage of thin membrane-like structures (a.k.a. webs) found in paper-handling, textile, sheet-metal and magnetic tapes industry. In this article, we examine the aero elastic stability of a web modeled as a uni-axially tensioned (along the machine direction) low aspect ratio Kirchhoff plate, which is subject to a fluid flow in the cross machine direction. Panel methods based on the distribution of singularity solutions (sources and doublets) on the surface of the web are used to numerically solve the problem of 3D unsteady potential flow surrounding the web. The equation of motion of the plate coupled to a fluid flow is discretized by using Galerkin's method. The discretization is performed in the configuration space formulation of the gyroscopic eigenvalue problem. The linear stability of this reduced order system is investigated. The onset of flutter instability as a function of base fluid flow in the cross machine direction is studied. The effects of fluid coupling on the frequencies and modes of oscillations of the web are also studied.

INTRODUCTION AND BACKGROUND

Thin membrane-like structures found in the paper-handling industry, textiles, thin sheet metals and magnetic tapes, often undergo breakage during their manufacture and processing stages. These flexible membranes or webs, which are transported through a series of rollers while remaining unsupported at their free edges, undergo large amplitude vibrations characterized as aero elastic flutter. This undesirable large amplitude motion and the ensuing possibility of breakage lead to poor manufacturing quality and considerable financial losses. Understanding the dynamics of such flexible structures with the intent of suppressing the undesirable motions is the primary goal of this work.

Several characteristic parameters play an important role in the vibrations of these webs. One characteristic parameter is the extremely low ratio of bending stiffness of the webs to the applied tension. Another characteristic property of such webs is their low density. The low density of such structures causes the surrounding air to easily influence the web motion. The effects of the surrounding air on the motion of the webs cannot be neglected. It is suspected that the air flows around the webs are a major cause of the fluttering motion of the webs. There are several reasons for the generation of air flows around the webs. For example in a printing process, when the web passes through a dryer, air is blown across the free edges (cross-machine direction) of the web. Apart from this, fluid viscosity coupled with web transport motion can generate air flows around the web. The primary goal of this research is to understand the mechanisms and determine the conditions that lead to the undesirable fluttering motion of the webs.

In this article, the vibrations of a uni-axially tensioned stationary web coupled to a surrounding incompressible and inviscid fluid flowing in the cross-machine direction is investigated. The linear stability of this aero elastic system is studied. Such an investigation about the aero elastic stability helps in understanding the conditions under which the web starts exhibiting fluttering motion. Apart from the conditions for the onset of flutter, this work also sheds light on the natural frequencies and the mode shapes of these webs for the various values of system parameters.

For a survey of the literature in the area of the transverse vibrations of axially moving structures without the fluid coupling, the reader is referred to the literature survey in the work of Vaughan [17]. A study regarding the effects of a surrounding incompressible and inviscid fluid on axially

moving paper webs can be found in the work of Raman *et al.* [13]. In this work, the web is modeled as a moving Kirchhoff plate with a very low bending stiffness to tension ratio. The effects of fluid coupling on the frequencies of the coupled system, especially the phenomenon of frequency clustering in paper webs, have been reported in this work.

The flutter phenomenon of stationary plates coupled to surrounding incompressible and inviscid fluid flows has been investigated by many researchers. Guo and Paidoussis [5] studied the linear stability of a rectangular plate immersed in a channel flow. This work assumes a two-dimensional beam model for the plate and does not capture the effects of the finite aspect ratio of the plate. Further, since their work does not model the trailing wake behind the plate, the system reported in Guo's work is conservative. An important aspect of the work presented in the current article is that it includes the effects of a trailing wake and along with it the inherent non-conservative nature of such a system.

The main motivation to study the problem on hand comes from experimentally observed flutter in webs when subjected to flows in cross-machine direction. Understanding the instability mechanisms could potentially lead to devising flutter suppression techniques for these important problems. The experimental results regarding the flutter observed in paper webs have been reported in the work of Hill [8] and Watanabe *et al.* [19]. Chang and Moretti [2] and Chang *et al.* [3] have presented several experiments on stationary and moving webs subjected to cross flow. Further, Chang and Moretti [4] also present a theoretical study by modeling the web as a tensioned infinitely wide Kirchhoff plate with base flow in the cross machine direction. Watanabe *et al.* [19] investigated the flutter of stationary paper sheets clamped only at the leading edge. Their work presents some interesting experimental observations along with theoretical modeling [20] to predict the onset of flutter.

Finally, the work presented by Vaughan [17] closely matches with the study presented in the present article. However, the fluid flow model presented in the former work did not include the effects of a trailing wake. These important effects have been included in the current article. A critical comparison between the fluid flow model in [17] and the one in the current work is discussed in later portions of this article.

The present article is organized in the following fashion. In the next section, the details of the model used for the web motion and the motion of the surrounding fluid have been presented. After that, the equations of motion are discretized by using Galerkin's method. Details on how to obtain the solution of the fluid flow problem by using the doublet-lattice method are presented next. The next section describes the effects of the trailing wake on the fluid-structure interaction. After this, a discussion on the computational issues pertaining to the problem on hand is given. Finally, we present the numerical results in the form of the eigenvalues of the coupled system. The effects of the base flow velocity on the frequencies and the mode shapes of the system along with the critical velocity for the onset of flutter are provided.

MODELING

The rectangular web is modeled as a flat, isotropic, linearly elastic and uni-axially tensioned Kirchhoff plate. The plate is located such that the right-handed Cartesian co-ordinate system $\{X, Y, Z\}$ has its origin at the center of the plate. The out-of-plane displacement $w(x, y, t)$ of the plate from its equilibrium state is governed by the following equation of motion

$$\rho w_{,tt} + D\nabla^4 w - N_{xx} w_{,xx} = f \tag{1}$$

where $(\,)_{,t}$ and $(\,)_{,x}$ stand for $\frac{\partial(\,)}{\partial t}$ and $\frac{\partial(\,)}{\partial x}$, respectively. ρ is the mass per unit area of the web and $D = \frac{Eh^3}{12(1-\mu^2)}$ is the bending stiffness of the plate. E is the Young's modulus of elasticity, h is the thickness of the web and μ is the Poisson's ratio. N_{xx} is the axial tension per unit width of the web applied along the X-direction. ∇^4 is the bi-harmonic operator and f represents the pressure force (due to the surrounding air) on the plate.

Figure 1 shows the plate, which has a length a along the X-axis and a width b along the Y-axis. The plate is supported by two roller supports as shown in Figure 1. Turnbull *et al.* [16] have shown that for small amplitude oscillations of tensioned beams with small bending stiffness to tension ratio, the roller supports can be suitably modeled as simple supports. Accordingly, the boundary conditions for the equation of motion are: simply-supported at the edges $x = a/2$ and $x = -a/2$ and free at the edges $y = b/2$ and $y = -b/2$.

The unsteady fluid flow in the 3D infinite domain surrounding the web is assumed to be incompressible. The existence of a thin wake (of negligible thickness) emanating from the trailing edge of the plate is also assumed. For small amplitude motion of the web, it is justified to restrict the wake to the X-Y plane. Such an assumption is popularly known in the literature as the linearized wake analysis [1]. The width of the wake is the same as that of the plate and it extends from the trailing edge of the plate to infinity downstream. The flow is assumed to be inviscid except in the thin layer comprising of the trailing wake. The continuity equation for the unsteady flow of an incompressible fluid is

$$\nabla \cdot u = 0 \tag{2}$$

where ∇ is the gradient operator and $u(x, y, z, t)$ is the velocity of the fluid. Since the flow field is irrotational (except in the thin wake where all the vorticity is concentrated), a scalar aerodynamic potential $\Phi(x, y, z, t)$, such that $u = -\nabla\Phi$, can be defined. The governing equation for the fluid flow then becomes

$$\nabla^2 \Phi = 0. \tag{3}$$

It is assumed that the fluid flow comprises of a steady base flow and small perturbations to this base flow caused by the web motion. The steady base flow has a velocity V along the Y-direction. The aerodynamic potential Φ can then be

conveniently divided into two parts ϕ^* and ϕ, where $\phi^* = -Vy$ is the aerodynamic potential that corresponds to the steady base flow and $\|\phi\| << 1$ is the perturbation aerodynamic potential caused by the plate motion. The perturbation potential ϕ must satisfy the continuity equation

$$\nabla^2 \phi = 0. \tag{4}$$

The boundary conditions for the fluid flow equations are derived by matching the normal velocity of the plate with the velocity of the fluid particle at that location. The velocity of a fluid particle in contact with the plate at location (x, y) is given by the material derivative of the plate displacement at the same location. Thus, on the plate surface, the following must be true

$$-\phi_{,z}\big|_{\text{on the plate}} = w_{,t} + Vw_{,y}. \tag{5a}$$

Additionally, it is required that the far field conditions be satisfied

$$\phi_{,n}\big|_{\text{as r}\to\infty} = 0 \tag{5b}$$

where $r = \sqrt{x^2 + y^2 + z^2}$ and n denotes any radial normal direction. The requirements in equations (5a) and (5b) become the boundary conditions for the perturbation potential ϕ.

The boundary conditions specified in equations (5a) and (5b) are purely kinematical in nature. The solution of the fluid flow problem obtained under these boundary conditions is in general not unique. The non-uniqueness of the solution is caused due to the yet undetermined value of the trailing edge vorticity that is shed into the wake [1]. An additional constraint popularly known in the literature as the "Kutta condition" is needed to find the value of the vorticity that is shed into the trailing wake. Once the trailing edge vorticity is known, the solution to the problem becomes unique. In the case of flow behind an oscillating plate, the Kutta condition can be interpreted [9] as requiring the pressure jump at the trailing edge of the plate to be zero, i.e.

$$\Delta p\big|_{\text{at the trailing edge}} = 0 \tag{6}$$

where $p(x, y, z, t)$ the pressure in the flow field and the symbol Δp refers to the difference between the values of pressure above and below the plate. Note that it is debatable as to whether the Kutta condition (which originally was formulated for the steady flow problems) can directly be extended to unsteady flow problems. However, there is some experimental evidence [9] to support such an assumption. Nevertheless, such an assumption about the validity of the Kutta condition has been made in this work and the results there of are analyzed.

Further, the perturbation aerodynamic potential is related to the pressure $p(x, y, z, t)$ in the flow field by Bernoulli's equation for unsteady flow

$$p(x, y, z, t) = \rho_{fluid}\left(\Phi_{,t} + V\Phi_{,y}\right). \tag{7}$$

The aerodynamic potential Φ can be divided into two parts; one which is symmetric about the plane Z=0 and the other which is anti-symmetric about the plane Z=0. The base flow potential ϕ^* is symmetric about the Z=0 plane and consequently does not cause any pressure differential on the plate. Only the anti-symmetric component of the perturbation aerodynamic potential ϕ will cause a pressure differential on the plate. Then, the pressure force $f(x, y, t)$ acting on the web is given by the difference in pressure acting on the lower and upper surfaces of the web

$$f(x, y, t) = 2\rho_{fluid}\left[\phi_{,t}(x, y, 0^+, t) + V\phi_{,y}(x, y, 0^+, t)\right] \tag{8}$$

where ϕ henceforth refers to only the anti-symmetric component of the perturbation potential.

Finally, following the work in [13], the equations of motion are non-dimensionalized in the following manner:

$$w' = w/a,\ x' = x/a,\ y' = y/a,\ z' = z/a$$

$$D = \frac{Eh^3}{12(1-\mu^2)},\ \varepsilon = \frac{D}{a^2 N_{xx}},\ t' = \frac{1}{a}\sqrt{\frac{N_{xx}}{\rho}}t,\ N'_{xx} = \frac{N_{xx}}{N_{xx}},$$

$$\kappa = \frac{b}{a},\ \Lambda = \frac{a\rho_{fluid}}{\rho},\ V' = \frac{V}{\sqrt{N_{xx}/\rho}},$$

$$\phi'(x', y', z', t') = \phi(x, y, z, t)\frac{1}{a\sqrt{N_{xx}/\rho}}.$$

Note that ε is the bending stiffness to tension ratio, Λ is the web density parameter and κ is the web aspect ratio. The primes denote the dimensionless quantities and are dropped in the subsequent analysis. The above non-dimensionalization results in the following set of equations for the fluid-structure interaction problem:

$$w_{,tt} + \varepsilon\nabla^4 w - w_{,xx} = 2\Lambda\left[\phi_{,t}(x, y, 0^+, t) + V\phi_{,y}(x, y, 0^+, t)\right]$$

$$\nabla^2 \phi = 0. \tag{9}$$

Accordingly, the non-dimensionalized boundary conditions are:

Plate Boundary Conditions:

a.) Simply supported at $x = 1/2, -1/2$

$$w(-1/2, y, t) = w(1/2, y, t) = 0,$$
$$w_{,xx}(-1/2, y, t) = w_{,xx}(1/2, y, t) = 0; \tag{10 a}$$

b.) Free edges at $y = \kappa/2, -\kappa/2$

$$
\begin{aligned}
&w_{,yy}(x,-\kappa/2,t) + \mu\, w_{,xx}(x,-\kappa/2,t) = 0,\\
&w_{,yy}(x,\kappa/2,t) + \mu\, w_{,xx}(x,\kappa/2,t) = 0,\\
&w_{,yyy}(x,-\kappa/2,t) + (2-\mu)\, w_{,yxx}(x,-\kappa/2,t) = 0,\\
&w_{,yyy}(x,\kappa/2,t) + (2-\mu)\, w_{,yxx}(x,\kappa/2,t) = 0;
\end{aligned}
\qquad (10\text{ b})
$$

Fluid Flow Boundary Conditions:

a.) Normal velocity matching

$$
-\phi_{,z}\big|_{\text{on the web}} = w_{,t} + V w_{,y}\,; \qquad (10\text{ c})
$$

b.) Far-field condition

$$
\phi_{,n}\big|_{\text{as r}\to\infty} = 0; \qquad (10\text{ d})
$$

c.) Kutta condition

$$
\Delta p\big|_{\text{at the trailing edge}} = 0. \qquad (10\text{ e})
$$

DISCRETIZED MODEL

The equations of motion in (9) are discretized using the Galerkin's method. The basis functions used for the discretization are the mass normalized in-vacuo (i.e. $\Lambda = 0$) eigenfunctions of a uni-axially and uniformly tensioned Kirchhoff plate. Thus we can write the web displacement as

$$
w(x,y,t) = \sum_{m=0}^{\infty}\sum_{n=0}^{\infty} q_{mn}(t)\Psi_{mn}(x,y). \qquad (11a)
$$

The discretization is performed in the configuration space formulation of the gyroscopic eigenvalue problem. Note that in equation (11a) $q_{mn}(t)$ represents the generalized coordinate of a basis function and the basis function $\Psi_{mn}(x,y)$ is given by

$$
\Psi_{mn}(x,y) = C_{mn}\sin\left[(m+1)\pi(x+1/2)\right]Y_{mn}(y)
$$

$$
m = 0,1,2...
$$

where

$$
\begin{aligned}
Y_{mn}(y) &= \cosh(\alpha_{mn1}y) + \gamma_{mn}\cosh(\alpha_{mn2}y) \qquad n = 0,2,4..\\
Y_{mn}(y) &= \sinh(\alpha_{mn1}y) + \gamma_{mn}\sinh(\alpha_{mn2}y) \qquad n = 1,3,5..
\end{aligned}
\qquad (11b)
$$

The values of $\alpha_{mn1}, \alpha_{mn2}$ and γ_{mn} depend on the eigenvalues of the boundary-value problem defined by the first equation in (9) and its corresponding boundary conditions, with $\Lambda = 0$ and $N_{xx} = 1$. Also note that C_{mn} is the mass normalized amplitude of the corresponding eigenfunctions.

Substituting the expansion in equation (11a) into the right-hand side of equation (10c) and assuming the time dependence of the perturbation potentials to be the same as that of the plate velocities, two boundary-value problems corresponding to the perturbation potentials ϕ_{mn1}(x,y,z) and ϕ_{mn2}(x,y,z) are obtained. The rationale is that each of the structural basis functions in equations (11) will drive the fluid flow and in turn give rise to two perturbation potentials: the first caused by matching the temporal part of fluid velocity (i.e. $w_{,t}$) and the second by matching the convective part of the fluid velocity (i.e. $Vw_{,y}$). Specifically, the two boundary-value problems arising from each basis function $\Psi_{mn}(x,y)$ are

$$
\nabla^2\phi_{mni} = 0;\ i = 1,2, \qquad (12)
$$

subject to the boundary conditions

$$
\begin{aligned}
\phi_{mn1,z}(x,y,0) &= \Psi_{mn}(x,y),\\
\phi_{mn2,z}(x,y,0) &= \Psi_{mn,y}(x,y).
\end{aligned}
\qquad (13)
$$

Note that the velocity matching in equation (13) is enforced on the Z=0 plane as against on the deformed web surface. This assumption can be shown to hold for small vibrations. Furthermore, under the assumption of small amplitude motion of the web, solutions of equations (12) and (13) for all the values of m and n can be added to obtain the total aerodynamic potential as

$$
\Phi(x,y,z,t) = \sum_{m=0}^{\infty}\sum_{n=0}^{\infty}\left\{\begin{matrix} q_{mn,t}(t)\phi_{mn1}(x,y,z) \\ \\ +Vq_{mn}(t)\phi_{mn2}(x,y,z)\end{matrix}\right\} - Vy. \qquad (14)
$$

While discretizing the equations by Galerkin's method, the expansion in equation (11a) is truncated to N x N terms and substituted in the left-hand side of the first equation in (9). Similarly, the expansion in equation (14) is truncated to N x N terms and substituted in the right-hand side of the first equation in (9). The resulting residual terms are weighted by using the basis functions $\Psi_{mn}(x,y)$ of equation (11a). After performing the integrations over the domain, the following discretized system of equations consisting of N x N equations is obtained:

$$
\begin{aligned}
&\{[I] + 2\Lambda[M_{air}]\}[\ddot{q}] + 2\Lambda V[C_{air}][\dot{q}]\\
&\qquad \{[K_1] + \varepsilon[K_2] + 2\Lambda V^2[K_{air}]\}[q] = 0
\end{aligned}
\qquad (15)
$$

where the matrices $[M_{air}]$, $[C_{air}]$ and $[K_{air}]$ represent the aerodynamic pressure forces in the form of added mass,

damping and added stiffness respectively. The matrices $[K_1]$ and $[K_2]$ represent the membrane stiffness and bending stiffness forces contributed by the structure.

It should be noted that the three matrices $[M_{air}]$,$[C_{air}]$ and $[K_{air}]$ corresponding to the aerodynamic loads are non-symmetric in nature. This is a direct consequence of the inclusion of the trailing wake in the fluid flow model. As a result, the coupled fluid-structure system is non-conservative in nature. The definitions of the various matrices in equation (15) are given in the appendix.

FLUID FLOW SOLUTION: THE DOUBLET-LATTICE METHOD

When evaluating the perturbation aerodynamic potential, a solution of the Laplace equation (i.e. equation 12) in a 3D infinite domain is sought. Vaughan [17] solved a similar problem using a numerical procedure in ANSYS. The solution methodology in that work is suited for problems with initially quiescent fluid flows. However, for base air flows, especially air flows in the cross-machine direction; it becomes necessary to include a trailing wake that ensures the uniqueness of the fluid flow solution. A numerical procedure best suited for handling such fluid flow problems should then be some variant of the vortex-lattice or the doublet-lattice method [9].

The doublet-lattice method used here is based on the use of Green's theorem [10]. The theorem states that the velocity potential at any point in the flow field can be expressed as an effect of sources and doublets distributed on the structure's surface. The solution methodology essentially consists of distributing singularity solutions of the Laplace equation on the surface of the web such that the boundary conditions in equations (13) are met. These methods of solving potential flow problems come under the category of boundary element methods.

Sources and doublets are elementary solutions of the Laplace equation. In order to evaluate the perturbation aerodynamic potential, doublet panels are distributed on the web as shown in Figure 2. The web is divided into R = P x Q doublet panels with P and Q panels along the X and Y direction, respectively. These doublet panels are located in the X-Y plane. At the geometric center of each panel, a control point is present. Apart from this, doublet wake panels are located on the downstream side as shown in Figure 2.

Denoting the unknown doublet strength of the i^{th} $(i = 1, 2, ...R)$ panel by Γ_i, a system of linear equations can be written as follows:

$$\begin{bmatrix} \beta_{11} & \cdots & \beta_{1R} \\ \vdots & & \vdots \\ \beta_{R1} & \cdots & \beta_{RR} \end{bmatrix} \begin{bmatrix} \Gamma_1 \\ \vdots \\ \Gamma_R \end{bmatrix} = \begin{bmatrix} \upsilon_1 \\ \vdots \\ \upsilon_R \end{bmatrix} \tag{16}$$

where β_{ij} $(i, j = 1, 2, ..., R)$ represents the velocity induced at the control point of the i^{th} panel by the j^{th} unit strength doublet panel. υ_i $(i = 1, 2, ..., R)$, which forms the right-hand side of equation (16) represents velocity that the fluid must have at the i^{th} control point. For example, when solving equation (12) subject to the first boundary condition in equation (13), the vector υ_i $(i = 1, 2, ...R)$ would consist of $\Psi_{mn}(x, y)$ evaluated at the i control points.

An important aspect of obtaining the fluid flow solution is modeling the doublet strength in the Z=0 plane off the web, especially in the trailing wake. As discussed earlier, since our interest lies only in finding the anti-symmetric component of the perturbation potential, the perturbation potential (and hence the doublet strength) is set to zero in the Z=0 plane everywhere except on the web and the trailing wake. On the surface of the web, the doublet strength is unknown and must be solved for as shown in equation (16). For modeling the doublet distribution in the wake, we follow the work of Von Kármán and Sears [18]. Assuming that the web is performing oscillatory motion with a circular frequency of ω, the vorticity generated on the web surface will be shed harmonically into the wake. This vorticity will be convected downstream with a steady base flow velocity V. Conventionally in steady flow problems, the Kutta condition is satisfied by matching the doublet strength of the last row of the structure panels with the first row of wake panels (See Figure 2). In doing so, the requirement in equation (10e) is automatically satisfied. However, for an unsteady flow problem like the present one, it is assumed that such a matching of doublet strengths takes place at every instant. Simply put, it is assumed that the Kutta condition is satisfied at every instant.

Now, if the web surface has velocities that perform an oscillatory motion of the type $e^{j\omega t}$, then the doublet distribution on the web surface would also have a similar harmonic behavior. Consequently, the distribution of doublet strength $\Gamma(x, y, t)$ in the wake would take the form

$$\Gamma(x, y, t) = \Gamma(x, y_{trailing\ edge})\, e^{-j\frac{\omega}{V}(y - y_{trailing\ edge})} e^{j\omega t},$$

where

$$\text{j}=\sqrt{-1}, \quad y_{trailing\ edge} = \kappa/2,$$
$$-1/2 \le x \le 1/2, \ \kappa/2 < \text{y} < \infty. \tag{17}$$

Such a distribution of doublet strength in the trailing wake was first suggested by Von Kármán and Sears. [18]. The work in reference [18] demonstrated the effect of the unsteadiness of airfoil motion on the trailing wake and in turn its effect on the fluid pressures exerted on the structure. However, these calculations were for a 2D unsteady flow and the ones described below in the current work correspond to a 3D unsteady flow.

The expression in (17) suggests that the distribution of doublet strength in the wake has two components with one leading the other by a phase of 90^o in time. Specifically, let us assume that the web surface velocity varies with time as $\cos(\omega t)$ and that we are interested in the fluid flow solution caused by this web surface velocity. Then the first component of the doublet wake distribution in phase with the web surface velocity would be $\Gamma(x, \kappa/2)\ \cos(\omega(y - \kappa/2)/V)\cos(\omega t)$ and the second one lagging behind by a 90^o phase would be $\Gamma(x, \kappa/2)\ \sin(\omega(y - \kappa/2)/V)\sin(\omega t)$. Now, these two wake

distributions are responsible for two fluid flow solutions, one lagging the other by a phase of 90°. Keeping this in mind, the fluid flow problem is solved in the following fashion.

Using the $\Gamma(x,\kappa/2)\cos(\omega(y-\kappa/2)/V)\cos(\omega t)$ distribution in the wake, with $\Gamma(x,\kappa/2)$ unknown at this stage, the left-hand side of equation (16) is modified. For a theoretical background on how the presence of a wake modifies the left-hand side of the set of linear equations in (16), the reader is referred to the monograph by Katz and Plotkin [9]. Returning to the fluid flow solution, the velocity of the web (and hence the velocity of the fluid particles in contact with the web) is evaluated at the i control points and this gives us the right-hand side of equation (16). The solution of equation (16) gives us the doublet strength $\Gamma(x,y)$ on the web, where x and y are such that $-1/2 \le x \le 1/2$ and $-\kappa/2 \le y \le \kappa/2$. This doublet distribution, which is based on a cosine distribution in the wake, is called $\Gamma_{cosine}(x,y)$. In other words, with this doublet distribution, the fluid flow solution in phase with the web surface velocity is obtained. In doing so, the trailing edge vorticity $\Gamma(x,\kappa/2)$ gets determined.

Now, since $\Gamma(x,\kappa/2)$ is known, we can find the influence of the second component of the wake. The distribution of $\Gamma(x,\kappa/2)\sin(\omega(y-\kappa/2)/V)\sin(\omega t)$ in the wake will cause some fluid flow at the i control points. This downwash caused by the second component of the wake must be nullified so that the no-penetration boundary condition on the web surface is always satisfied. Thus, a doublet distribution on the web that nullifies the influence of the second wake component is determined. This doublet distribution called $\Gamma_{sine}(x,y)$ (which lags the velocity of the web surface by a 90° phase) corresponds to the fluid flow lagging the web surface velocity by a 90° phase.

The two doublet distributions $\Gamma_{cosine}(x,y)$ and $\Gamma_{sine}(x,y)$ will give rise to two perturbation potentials $\phi_{cosine}(x,y,z)$ and $\phi_{sine}(x,y,z)$. These two perturbation potentials can be combined to obtain a single response perturbation potential $\phi(x,y,z)$ that lags the velocity causing it by the corresponding phase angle. In summary, in the absence of a trailing wake, the response aerodynamic perturbation potential $\phi(x,y,z)$ and the web surface velocity causing it would have been in phase with one another. The presence of a trailing wake makes the response perturbation potential $\phi(x,y,z)$ to lag the velocity of the web surface by some phase angle.

Tang *et al.* [14] have performed calculations for a 3D flow around a cantilevered plate using a time-stepping unsteady vortex-lattice method along with some reduced order modeling techniques. The difference between the fluid flow solution in the work of Tang *et al.* [14] and the current work is that the former is applicable to a more general class of problems including those with the non-linear aerodynamic effects. Essentially, unlike the fluid model in the current work, Tang *et al.* [14] do not make any restricting assumptions about the small amplitude motion of the fluid caused by a small amplitude web motion. The large amplitude motion of the fluid can capture the non-linear aerodynamics. An assumption that the response perturbation potential follows the web motion harmonically is possible only for small amplitude web motions. Such an assumption allows the fluid flow solution by the frequency-domain methods which take smaller computational effort by orders of magnitude when compared to a time-stepping vortex-lattice method [6].

Returning to the harmonic wake distribution, we now examine the effects of such a wake distribution on the pressure loading on the plate. In the work of Vaughan [17], the trailing wake was absent and the flow calculations corresponded to a zero circulation solution. The perturbation potential solution $\phi(x,y,z)$ was in phase with the web surface velocity. On substitution into the right-hand side of equation (7), this gave rise to an added mass pressure force, two gyroscopic pressure forces and one added stiffness force. These forces lead the web displacement by 180^0, 90^o and 0^o respectively. With the additional trailing wake, the perturbation potential solution $\phi(x,y,z)$ would lag behind the web surface velocity which caused it. Due to this extra phase lag, the magnitudes of the added mass, gyroscopic and stiffness forces would change. Furthermore, the aerodynamic forces proportional to the web surface velocity, which were conservative gyroscopic in nature, become non-conservative. For a detailed discussion on how the magnitude and the phase of pressure forces change with the inclusion of a trailing harmonic wake, the reader is referred to the work of Von Kármán and Sears.[18].

EFFECTS OF THE WAKE AND THE P-K METHOD

In a 3D potential flow calculation around a structure with a sharp edge, the presence of a trailing wake renders the fluid flow solution unique. But including a harmonically varying trailing wake makes the linear stability analysis even more involved. The natural frequencies, the mode shapes and the linear stability of the coupled fluid-structure system can only be ascertained if the pressures forces acting on the web can be calculated. For calculating the fluid pressure forces, one needs to solve the fluid flow problem. However, as is clear from the expression in equation (17), the fluid flow solution depends on the doublet strength distribution in the trailing wake and the ω involved there in is *a priori* not known. In other words, the matrices $[M_{air}]$, $[C_{air}]$ and $[K_{air}]$ (representing the aerodynamics in the form of the added mass, damping and stiffness forces), which will be used in calculating the natural frequencies ω of the coupled system, themselves depend on ω. Such a system where the aerodynamic forces depend on as well as decide the value of ω, calls for the implementation of an iterative procedure, which starts with an initial guess for ω, computes the aerodynamic forces and in turn uses them to better estimate the value of ω until a converged answer is achieved.

Moreover, due to the inclusion of a trailing wake, the system becomes non-conservative, i.e. the $[M_{air}]$, $[C_{air}]$ and $[K_{air}]$ matrices in equation (15) become non-symmetric. Also, unlike a conservative gyroscopic system, the $[C_{air}]$ matrix has non-zero entries on the diagonal. Due to the non-conservative nature of the system, the motion of the web will in general be either decaying or growing in time. This

further aggravates the problem because if the motion of the web is decaying or growing, then the assumption of a harmonically varying wake (refer to equation (17)) and the aerodynamic pressures predicted by it might not be correct. Then, for calculating the frequencies and the associated rate of decay/growth for such a non-conservative system, we need to use the "p-k method" presented by Hassig [7].

In the current work, the p-k method has been used. First, following the work of Theodorson [15], a reduced frequency $k = \omega/V$ is defined. Then, assuming the web motion to be in the form of a particular basis function Ψ_{mn}, the fluid flow solution is computed over a range of values for the reduced frequency k. Notice that a change in the value of k changes the trailing wake influence and hence leads to a different fluid flow solution. This procedure is repeated for all the basis functions used in the Galerkin expansion. Thus, over a range of the values of $k = \omega/V$, we have the solutions for the perturbation potentials arising due to the entire set of basis functions. Further, using the equations in the appendix, the aerodynamic matrices $[M_{air}]$, $[C_{air}]$ and $[K_{air}]$ are computed. At the end of this step, we would have the aerodynamic pressure forces $[M_{air}]$, $[C_{air}]$ and $[K_{air}]$ as a function of the reduced frequency k. Having computed the aerodynamic forces over a range of reduced frequencies, we need to use these to find the natural frequencies of the coupled system. The iterative procedure for doing the same is briefly described below.

For a given base flow velocity V, the iteration starts by guessing the value of ω followed by a computation of the reduced frequency $k = \omega/V$ and the corresponding aerodynamic matrices. Using these matrices in equation (15), we solve the determinant for the values of ω. The roots of the determinant are complex numbers with the real part representing the oscillation frequency and the imaginary part representing the rate of growth. At the end of first iteration, the frequencies of the system can be obtained as $\omega_1 = \omega_{\text{Real1}} - j\omega_{\text{Imag1}}$. Neglecting the imaginary part, the aerodynamic matrices can be recalculated using the value ω_{Real1} only to obtain a better approximation $\omega_2 = \omega_{\text{Real2}} - j\omega_{\text{Imag2}}$. During every such iteration, the imaginary part ω_{Imag} of the frequency, which represents the rate of growth, is neglected. Note that such an approach will only work if the value of ω_{Imag} is small compared to ω_{Real}. The argument behind using this method is that if $\omega_{\text{Imag}} << \omega_{\text{Real}}$, then the web motion is decaying or growing very slowly when compared to its oscillations. In that case, the aerodynamic loads based on a constant amplitude harmonic motion should be able to predict aerodynamics for slowly increasing or slowly decaying web motions [7].

COMPUTATIONAL ISSUES

For the numerical results presented in this paper, a web aspect ratio $\kappa = 1$ is chosen. The calculations were performed for a web with the following numerical values for the various constants:

$a = b = 1.372$ m, $h = 25.4 \times 10^{-6}$ m, $E = 6.8\ GPa$
$\mu = 0.3$, $N_{xx} = 100$ N/m, $\rho = 40$ g/m^2 and $\rho_{fluid} = 1.225$ kg/m^3.

Also since the web motion is symmetric about the Y-axis, the fluid flow computations are performed for only one-half of the plate. Thus, there are 50 doublet panels along the positive X-axis and 100 doublet panels along the Y-axis. In all there are 5000 control points over one-half of the plate. At each of these control points the velocity of the web and the fluid are matched. A convergence study with respect to the number of required control points was performed and the results are shown in Figure 3. The results in Figure 3 demonstrate how the Galerkin projection of the added mass pressure force on the 1st and the 6th basis function changes with the number of control points. Obviously, if one desires to use a large number of basis functions, then the basis functions corresponding to the higher frequencies would have rapidly changing spatial behavior. In that case, more control points are needed for capturing the spatial gradients of the higher basis functions. For the purpose of the present problem, a moderate number of basis functions were chosen. For the first 12 basis functions, a choice of 5000 control points seems satisfactory. From Figure 3 it is clear that inclusion of a larger number of control points is not necessary and would increase the computational time by an order of magnitude to achieve a marginal gain in accuracy.

Another important computational issue is about the number of wake panels used in the computation. Although theoretically, the wake extends downstream from the trailing edge of the plate till infinity, in a numerical scheme it needs to be terminated at a finite distance from the trialing edge. As a result, the wake panels are arranged starting from the trailing edge of the plate till a distance equal to 3 times the plate length. After this length, the wake is represented by straight lines parallel to the steady base flow. Care must also be exercised in deciding the wake panel density i.e. the number of wake panels present per unit wake length along the downstream direction. Considering the wake panel density is especially important for higher values of the reduced frequency k because at these values of k, the wake strength is changing rapidly.

The convergence properties of the frequencies predicted by the Galerkin method are also studied and presented in Figure 4. The top portion of Figure 4 shows the convergence of the rate-of-growth as the number of basis functions is changed. Note that these calculations were performed for the first mode for a cross-flow non-dimensional velocity of 0.03. Likewise, the lower portion of Figure 4 shows the convergence characteristics of the frequency of the first mode as more and more basis functions are added.

Finally, before presenting numerical results corresponding to the stability of the coupled system, the results given by the doublet-lattice method need to be benchmarked. Towards this end, the added mass pressure force for a rigid plate oscillating in a stationary fluid was calculated. Meyerhoff [11] calculates the non-lifting potential around a rigid plate oscillating in a fluid by distributing point doublets of unknown strength on the plate. The added mass forces predicted by Meyerhoff and the ones given by the constant strength doublet-lattice method are in excellent agreement with one another.

NUMERICAL RESULTS AND ANALYSIS

The numerical values for various constants are given in the previous section. Note that these values of tension and bending stiffness lead to an ε value that is of the order of 10^{-8}. However, for such low values of ε, the basis functions with very high value of n lose stability before those with lower nodal lines along the X-direction. From the point of view of convergence, in order to accurately predict the frequencies for such high modes, it would be required to use a very large number of basis functions. Instead, following the work of Vaughan [17], calculations were performed at an artificially high ε value of 5×10^{-6}.

In these calculations, the basis functions used correspond to the values of $m = 0$ and n=0,1,2,...,12. Using the p-k method described in the previous section, the frequencies of the coupled system as a function of non-dimensionalzed cross-flow velocity are found and shown in Figure 5. Note that the frequencies corresponding to the first five modes have been shown. The corresponding rates-of-growth are shown in Figure 6. A remarkable feature of the frequency plots is the occurrence of the curve veering phenomenon. The veering effect can be verified by performing a convergence study (by including more and more basis functions) of the coupling factors between two veering modes in the neighborhood of suspected veering [12].

As the flow velocity is increased, the frequency of oscillation for all the modes decreases. An important feature of this coupled fluid-structure problem is its non-conservative nature. Even in the absence of structural damping, the system displays decaying motion when the base flow velocity is below the critical velocity. As a result, the rate-of growth plot is negative for all the modes.

Note that the natural frequencies of the web when $V = 0$ are known and the lowest five are shown in Figure 5. The corresponding rate-of-growth is zero, which indicates a conservative system. The natural frequencies of the web corresponding to the base velocity range of 0-0.02 have not been calculated. The reason for this is that for such low values of V, the reduced frequency $k = \omega / V$ assumes very large values and the aerodynamic matrices corresponding to these values of k were not computed. In the section on p-k method, it was mentioned that the $[M_{air}]$, $[C_{air}]$ and $[K_{air}]$ aerodynamic matrices were computed for all the basis functions over a range of the reduced frequency k. The range of values of k used was 0-100. This choice of the range of reduced frequency was dictated purely by the computational time involved. It seems unnecessary to calculate aerodynamic loads for very high values of k. The rationale behind this is that doing so would only help in accurately predicting the natural frequencies at very low base velocities where the chances of flutter are small.

The rates-of-growth in Figure 6 are very close to one another. An enlarged version of the same plot is shown in the upper portion of Figure 6. It can be seen that till the non-dimensional velocity of V=0.0471, all the modes have a negative rate-of-growth indicating a stable system. At the non-dimensional velocity of V=0.0471 (this corresponds to an actual velocity of V=0.2453 m/s), the rate-of-growth of the second mode becomes positive, which indicates a flutter instability. Following this, at velocities V=0.052 (V=0.2707 m/s) and V=0.054 (V=0.2811 m/s), the third and the first mode lose stability respectively and start fluttering. Further at non-dimensional velocity V=0.074 (V=0.3853 m/s), the first mode loses stability by divergence. When the divergence instability occurs, the rate-of-growth for the first mode splits into two different solutions as shown in Figure 6.

A closer observation of Figure 5 and 6 reveals that mode 2, which starts fluttering first, does so when the frequencies of mode 2 and mode 3 come very close to one another. Also as seen in Figure 6, just when the rate-of-growth of mode 2 crosses to the positive side, the rate-of-growth of mode 3 turns downwards and starts decreasing. It is unclear at this stage as to whether these frequencies would come even closer on inclusion of more basis functions in the Galerkin expansion. Such a study as to whether or not the two modes coalesce when more basis functions are included is beyond the scope of this article and remains as future work.

At this stage, it is appropriate to reexamine the validity of the assumptions made while using the p-k method. For example, for the first mode, the frequency of oscillation at non-dimensional velocity V=0.04 is 0.58256 rad/s and the corresponding rate of growth is -0.00289. This means that the rate at which the web motion is decaying is an order of magnitude less when compared to the oscillatory motion of the web. Since the web motion is decaying slowly, the assumptions made about the p-k method are valid.

Another important observation that needs to be made is that about the effects of including the trailing wake in the model. The model used in the work of Vaughan [17] does not include the trailing wake and this results in a conservative gyroscopic system which first loses stability at non-dimensional velocity V=0.0689 by divergence. At higher velocities, flutter instabilities are found to occur through the phenomenon of mode coalescence. However, inclusion of the trailing wake makes the system non-conservative. Furthermore, the flutter instability is seen to occur first at a lower non-dimensional velocity of V=0.0471 even before the divergence instability happens.

The web starts fluttering at the critical velocity of V=0.0471. Shown in Figure 7 are nine different instants of the motion of the web (V=0.0471) as it completes one cycle of oscillation. Figure 8 shows the shape of the web (along the line $x = 0$) for nine different instants as it completes one cycle of oscillation. It can be seen that compared to the trailing edge, the amplitude of motion of the leading edge is almost twice as large as the trailing edge. Furthermore, the large amplitude motion of the leading edge travels downstream like a wave though the web structure.

FUTURE WORK AND CONCLUSION

In this work, the linear stability of a stationary web coupled to base air flow in the cross-machine direction was investigated. The analysis revealed some interesting dynamical characteristics such as occurrence of flutter instability before the divergence instability. This work shows that the flutter mode of these webs is characterized by significant motion of the leading edge. This work demonstrated that including a wake emanating from the trailing edge of the plate makes the system non-conservative.

One of the immediate goals for this problem is to perform a rigorous convergence analysis with regards to the number of basis functions used. Such a convergence study would help in resolving the veering phenomenon along with answers to questions such as: whether the modes coalesce before fluttering etc. It should be noted that the current work does not include a wake vortex sheet emanating from the leading edge of the plate. As a result, the fluid flow solution is singular at the leading edge. An important problem is to study the effect of a vortex wake sheet emanating from the leading edge of the plate. After this the linear stability problem can be analyzed for different aspect ratios and different values of the number ε. Another long-term goal of this research is to investigate the post-flutter dynamics of this system by using non-linear structural equations with suitable non-linear behavior included in the fluid flow model as well. The doublet-lattice method used in this work would then be modified to a panel method that can capture the non-linear fluid-structure interaction. Towards that end, the tools developed in the current work certainly hold a promise for solving the non-linear fluid-structure interaction problem.

ACKNOWLEDGMENTS

This work was funded by the grant from the National Science Foundation [CAREER AWARD # 0116414-CMS].

REFERENCES

[1] Bassanini, P., Casciola, C. M., Lancia, M. R., and Piva, R., 1996, "On the Trailing Edge Singularity and Kutta Condition for 3D airfoils," *European Journal of Mechanics, B/Fluids*, 15(6), pp. 809-830.

[2] Chang, Y. B., and Moretti, P. M., 1992, "An Experimental Study on Edge Flutter in Webs," *Applied Mechanics Division –Proceedings of the ASME*, 149.

[3] Chang, Y. B., Cho, H. C., and Moretti, P. M., 1999, "Edge Flutter," *Noise Control and Acoustics Division – Proceedings of the ASME*, 26, pp. 413-423.

[4] Chang, Y. B., and Moretti, P. M., 2002, "Flow-Induced Vibration of Free Edges of Thin Films," *Journal of Fluids and Structures*, 16(7), pp. 989-1008.

[5] Guo, C. Q., and Paidoussis, M.P., 2000, "Stability of Rectangular Plates with Free Side-Edges in Two – Dimensional Inviscid Channel Flow," *ASME Journal of Applied Mechanics*, 67(1), pp. 171-176.

[6] Hall, K. C., 1994, "Eigenanalysis of Unsteady Flows about Airfoils, Cascades, and Wings," *AIAA Journal*, 32(12), pp. 2426-2432.

[7] Hassig, H. J., 1971, "An approximate True Damping Solution of the Flutter Equation by Determinant Iteration," *Journal of Aircraft*, 8(11), pp. 885-888.

[8] Hill, K. C., 1988, "Dryer Sheet Stability for Older Paper Machines," *Tappi Journal*, 71, pp. 55-59.

[9] Katz, J., and Plotkin, A., 2001, *Low Speed Aerodynamics*, Cambridge University Press.

[10] Lamb, H., 1932, *Hydrodynamics*, Dover, New York.

[11] Meyerhoff, W. K., 1970, "Added Mass of Thin Rectangular Plates Calculated from Potential Theory," *Journal of Ship Research*, 14, pp. 100-111.

[12] Perkins, N. C., and Mote, C. D., 1986, "Comments on Curve Veering in Eigenvalue Problems," *Journal of Sound and Vibration*, 106(3), pp. 451-463.

[13] Raman, A., Wolf, K.D., and Hagedorn, P., 2001, "Observations on the Vibrations of Paper Webs," *Proceedings of the International Conference on Web Handling*, Stillwater, OK.

[14] Tang, D., Dowell, E. H., and Hall, K. C., 1999, "Limit Cycle Oscillations of a Cantilevered Wing in Low Subsonic Flow," *AIAA Journal*, 37(3), pp. 364-371.

[15] Theodorson, T., 1935, "General Theory of Aerodynamic Instability and the Mechanism of Flutter," *NACA Report* 496.

[16] Turnbull, P. F., Perkins, N. C., and Schultz, W. W., 1995, "Contact-Induced Non-linearity in Oscillating Belts and Webs," *Journal of Vibration and Control*, 1, pp. 459-479.

[17] Vaughan, M., 2003, *Aero elastic Stability of Axially Moving Webs Coupled to Incompressible Flows*, Master's Thesis, Purdue University, IN, USA.

[18] Von Kármán, T., and Sears, W. R., 1938, "Airfoil Theory for Non-Uniform Motion," *Journal of Aeronautical Sciences*, 5(10), pp. 379-390.

[19] Watanabe, Y., Suzuki, S., Sugihara, M., and Sueoka, Y., 2002, "An Experimental Study of Paper Flutter," *Journal of Fluids and Structures*, 16(4), pp. 529-542.

[20] Watanabe, Y., Isogai, K., Suzuki, S., and Sugihara, M., 2002, "A Theoretical Study of Paper Flutter," *Journal of Fluids and Structures*, 16(4), pp. 543-560.

FIGURES

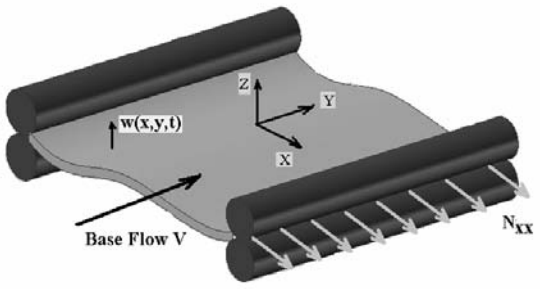

Figure 1 A Schematic for the uni-axially tensioned stationary web coupled to cross-machine base flow

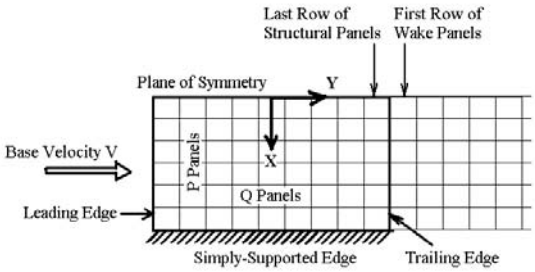

Figure 2 A schematic representation of the doublet-lattice method showing the arrangement of doublet panels on the plate and in the wake

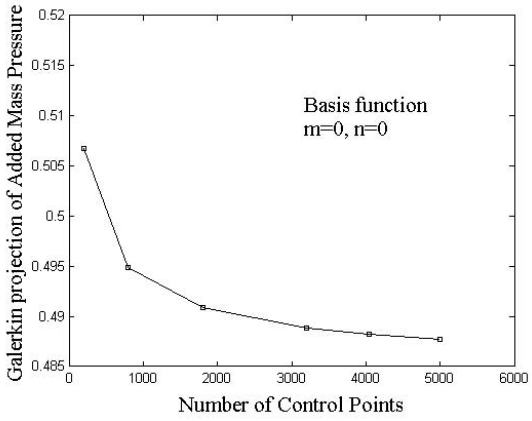

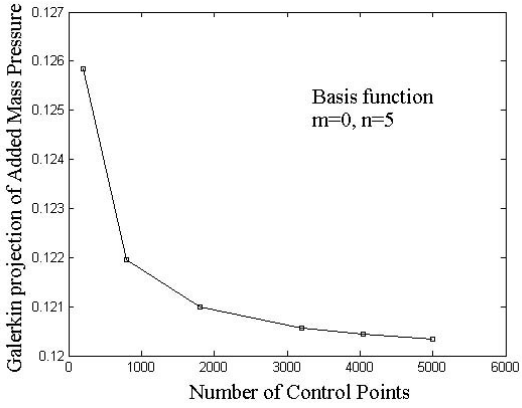

Figure 3 Convergence of the Pressure Force as the Control Points in the Doublet-Lattice method are increased.

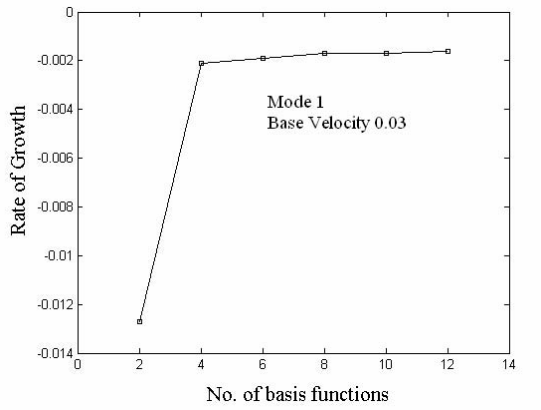

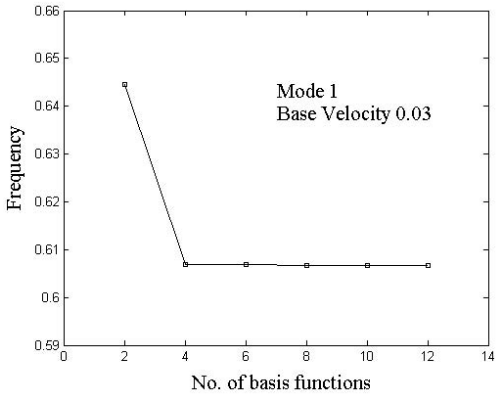

Figure 4 Convergence of the Frequency and the Rate of Growth as the number of Basis Functions is increased.

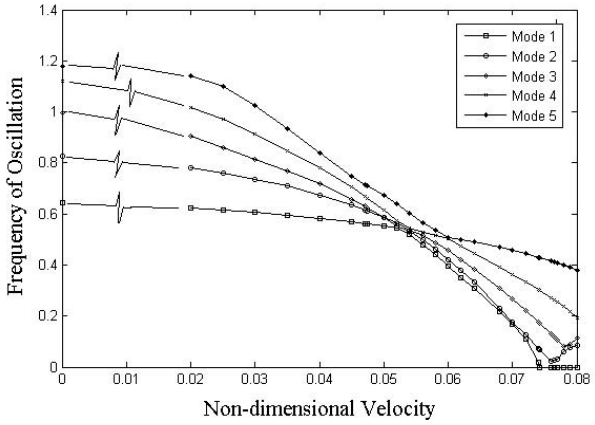

Figure 5 Variation of the natural frequencies of the first five modes with change in the base flow velocity.

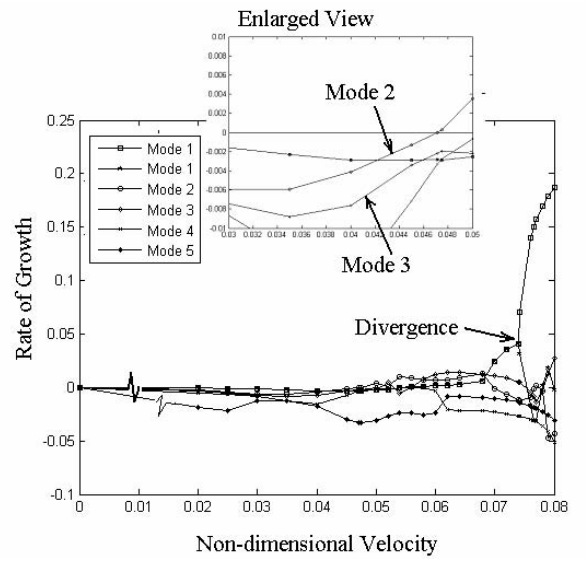

Figure 6 Variation of the rate of growth of the first five modes with the change in the base flow velocity.

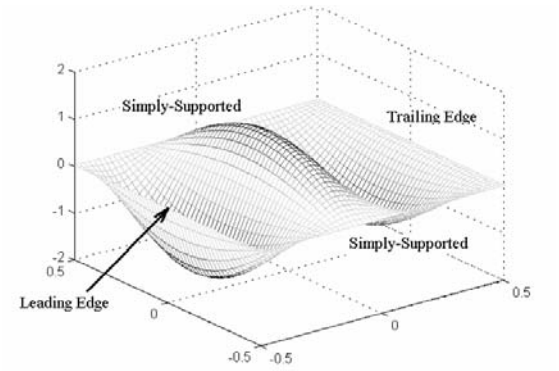

(a) $t = 2\pi / 9\omega$

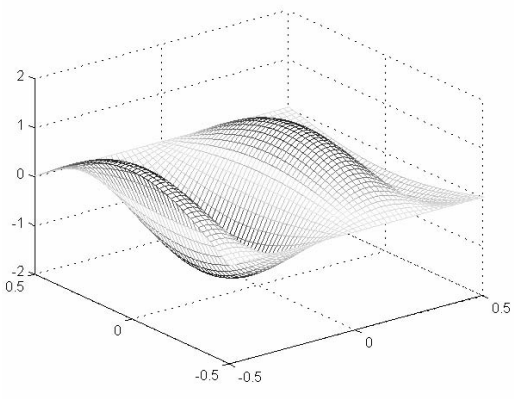

(d) $t = 8\pi / 9\omega$

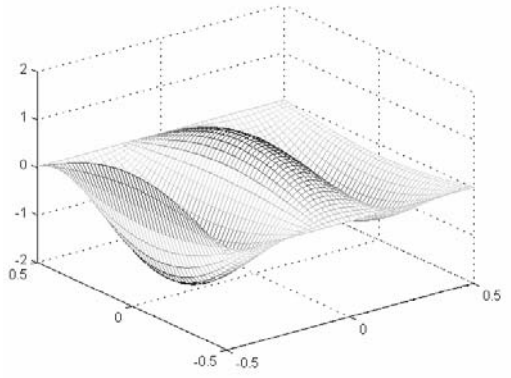

(b) $t = 4\pi / 9\omega$

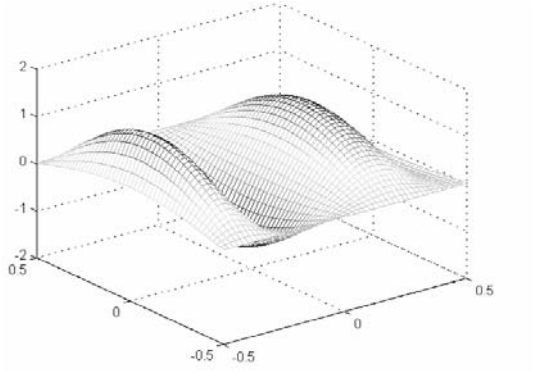

(e) $t = 10\pi / 9\omega$

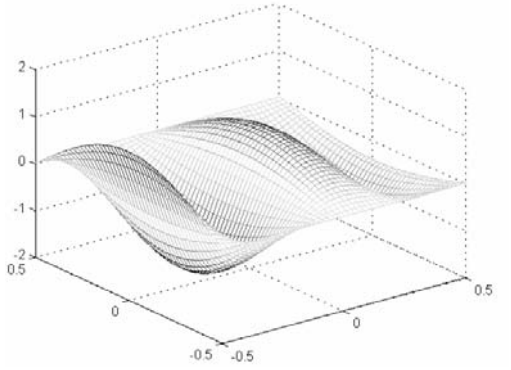

(c) $t = 2\pi / 3\omega$

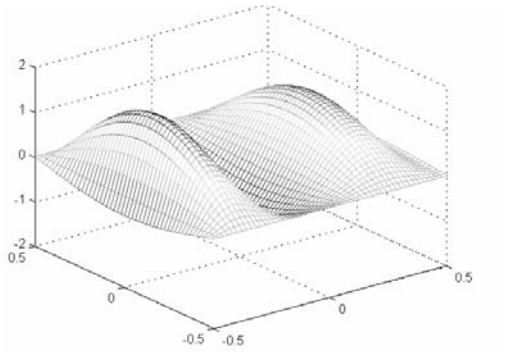

(f) $t = 4\pi / 3\omega$

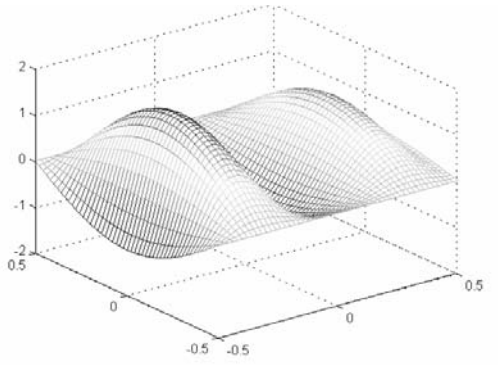

(g) $t = 14\pi / 9\omega$

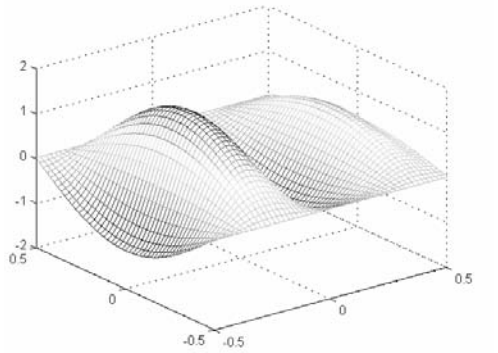

(h) $t = 16\pi / 9\omega$

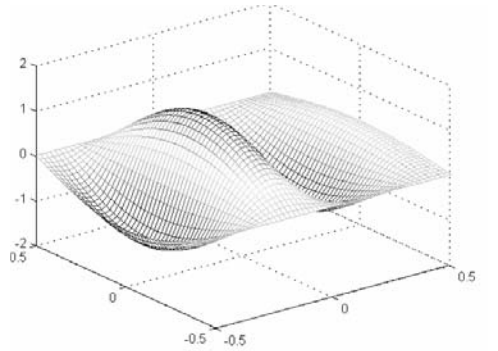

(i) $t = 2\pi / \omega$

Figure 7 The shape of the web at nine different instants during one cycle of oscillation at the onset of flutter.

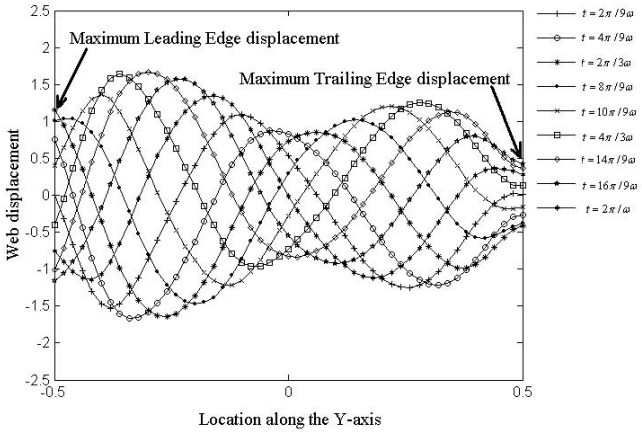

Figure 8 The shape of the web along the line x=0 for nine different instants during one cycle of oscillation at the onset of flutter.

APPENDIX

The definitions of the various matrices in equation (15) are as follows:

$[I]$ is the N x N identity matrix;

$$(M_{air})_{ij;mn} = 2\int_{x=0}^{0.5}\int_{y=-\kappa/2}^{\kappa/2} \psi_{ij}(x,y)\ \phi_{mn1}(x,y,0^+)\ dxdy;$$

$$(G_{air})_{ij;mn} = 2\int_{x=0}^{0.5}\int_{y=-\kappa/2}^{\kappa/2} \psi_{ij}(x,y) \begin{bmatrix} \phi_{mn1,y}(x,y,0^+) \\ +\phi_{mn2}(x,y,0^+) \end{bmatrix} dxdy;$$

$$(K_{air})_{ij;mn} = 2\int_{x=0}^{0.5}\int_{y=-\kappa/2}^{\kappa/2} \psi_{ij}(x,y)\ \phi_{mn2,y}(x,y,0^+)\ dxdy;$$

$$(K_1)_{ij;mn} = \int_{x=-0.5}^{0.5}\int_{y=-\kappa/2}^{\kappa/2} \psi_{ij,x}(x,y)\ \psi_{mn,x}(x,y)\ dxdy;$$

$$(K_2)_{ij;mn} = \int_{x=-0.5}^{0.5}\int_{y=-\kappa/2}^{\kappa/2} \begin{Bmatrix} \psi_{ij,xx}(x,y)\ \psi_{mn,xx}(x,y) \\ +\ \psi_{ij,yy}(x,y)\ \psi_{mn,yy}(x,y) \\ +2(1-\mu)\psi_{ij,xy}(x,y)\ \psi_{mn,xy}(x,y) \\ +\ \mu\psi_{ij,xx}(x,y)\ \psi_{mn,yy}(x,y) \\ +\ \mu\psi_{ij,yy}(x,y)\ \psi_{mn,xx}(x,y) \end{Bmatrix} dxdy.$$